

Graph Convolutional Networks for Multi-modality Medical Imaging: Methods, Architectures, and Clinical Applications

Authors: Kexin Ding¹, Mu Zhou², Zichen Wang^{3,4}, Qiao Liu⁵, Corey W. Arnold^{3,4}, Shaoting Zhang⁶, Dimitri N. Metaxas⁷

¹Department of Computer Science, The University of North Carolina at Charlotte, Charlotte, USA

²Sensebrain Research, San Jose, USA

³Computational Diagnostics Lab, UCLA, Los Angeles, USA

⁴Department of Bioengineering, UCLA, Los Angeles, USA

⁵Department of Statistics, Stanford University, Stanford, USA

⁶Sensetime Research and Shanghai AI laboratory, Shanghai, China

⁷Department of Computer Science, Rutgers University, New Jersey, USA

**Corresponding to Shaoting Zhang (zhangshaoting@sensetime.com) and Dimitris N. Metaxas (dnm@cs.rutgers.edu)*

Abstract

Image-based characterization and disease understanding involve integrative analysis of morphological, spatial, and topological information across biological scales. The development of graph convolutional networks (GCNs) has created the opportunity to address this information complexity via graph-driven architectures, since GCNs can perform feature aggregation, interaction, and reasoning with remarkable flexibility and efficiency. These GCNs capabilities have spawned a new wave of research in medical imaging analysis with the overarching goal of improving quantitative disease understanding, monitoring, and diagnosis. Yet daunting challenges remain for designing the important image-to-graph transformation for multi-modality medical imaging and gaining insights into model interpretation and enhanced clinical decision support. In this review, we present recent GCNs developments in the context of medical image analysis including imaging data from radiology and histopathology. We discuss the fast-growing use of graph network architectures in medical image analysis to improve disease diagnosis and patient outcomes in clinical practice. To foster cross-disciplinary research, we present GCNs technical advancements, emerging medical applications, identify common challenges in the use of image-based GCNs and their extensions in model interpretation, large-scale benchmarks that promise to transform the scope of medical image studies and related graph-driven medical research.

1. Introduction

Graph representation has been extensively studied in information extraction, relational representation, and multi-modality data fusion^{1, 2, 3} applications. The rich topological and spatial characteristics of graphs essentially uncover differential relations among individual graph elements⁴. In medical image analysis, the diverse shape, anatomy, and appearance information provide a key data source to characterize the interactions among the diagnostic region of interests (ROIs) and reveal disease status⁵. Therefore, image-based graph modeling and inference can deepen our understanding of the complex relational patterns hidden in disease tissue regions. The recent surge in the use of graph convolutional networks (GCNs), a branch of deep learning characterized by graph-level model development, has brought a new wave of information fusion techniques through their widespread applications in medical imaging, ranging from disease classification⁶ and tumor segmentation⁷, to patient outcomes prediction⁸.

Graph convolutional networks (GCNs) explore the heterogeneous graph data via a series of graph-level convolutions, sampling, and enable model inference on both graph node attributes and relational structures⁴. The development of GCNs extends conventional graph embedding methods (e.g., Deepwalk⁹ and node2vec¹⁰) by generating a low-dimensional graph representation without considering node attributes. In addition, GCNs have resulted in multifaceted advances on feature extraction, data fusion, and interpretability. First, GCNs extract multi-scale spatial image data relations by characterizing inter- and intra-distances between features from different tissue regions, which are vital for understanding disease characterization and severity assessment¹. Further, GCNs can fuse heterogeneous cross-modality data, e.g., imaging and non-imaging data. The cross-modality analysis is of substantial interest since it can improve our understanding of disease mechanisms and diagnosis compared to the use of single modality data. For instance, the fusion of functional magnetic resonance imaging (fMRI) data and clinical records can provide auxiliary benefits for brain disease analysis¹¹. Similarly, an integrative analysis of multi-omics profiles and imaging patterns promises to discover novel image-to-genome associations for cancer biomarker discovery^{12, 13}. Finally, GCNs provide the possibility for model outcome interpretation by capturing the structural dynamics of complex graphs. The model outcome can visualize both node distributions and subgraph connectivity derived from the entire graph representation. In summary, GCNs have the potential to analyze large amounts of graph-level information which is crucial to advance medical imaging understanding and guide decision making in clinics.

A general pipeline for utilizing GCNs in medical imaging is shown in Fig. 1, which highlights key components of multi-modality imaging and clinical data, graph representation frameworks, and downstream clinical applications. To provide a guideline to foster cross-disciplinary research in the field of GCNs and medical imaging, the major contributions of this survey can be summarized as follows:

1. We outline current state-of-the-art GCNs that are widely used in medical image analysis. We summarize the underlying formulation, architectures and their variations, to advance graph-based medical imaging research.
2. We present the use of GCNs in radiological images, histopathology images, and other imaging modalities. We organize them in a unified taxonomy based on graph construction approaches and downstream clinical applications.
3. We offer insights into the image-to-graph transformation that is vital to determine the success of GCNs, including the modeling of graph components and different graph construction metrics. This review provides a key reference for researchers to explore the fast-growing synergy between graph architecture and medical imaging data.
4. Emerging opportunities and future directions are discussed in image-based GCNs and their extensions across multiple medical applications. These insights can greatly expand the scope of developing and using GCN approaches in medical imaging and related data-driven medical studies.

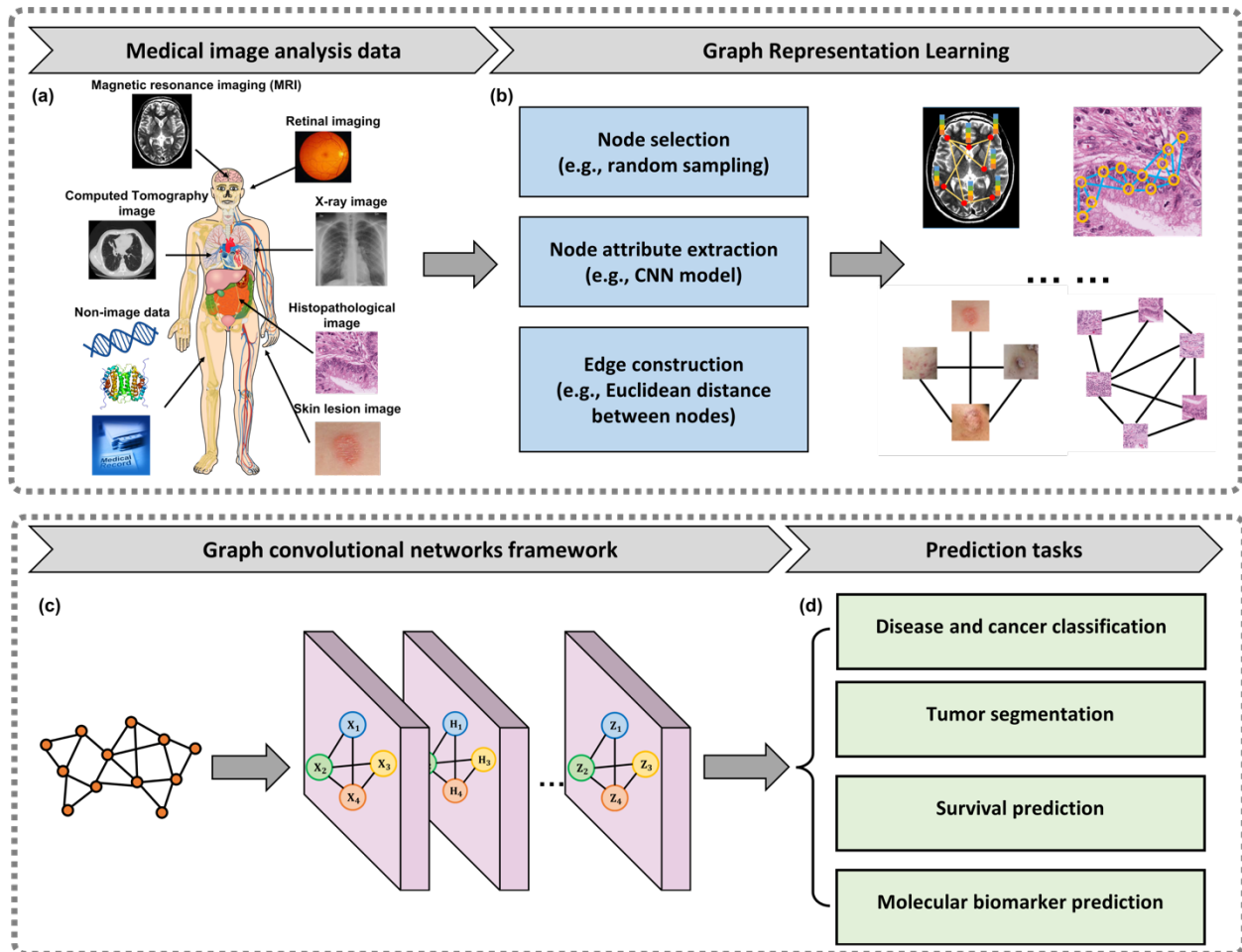


Fig. 1. A general pipeline for utilizing GCNs in medical image analysis. (a) Medical image analysis data. Multi-modality medical imaging and other non-image data can be jointly considered for GCN modeling and

analysis. **(b) Graph representation learning.** The image-graph transformation pipeline includes node selection, node attribute extraction, and edge construction. For different types of medical images, we aim to design a variety of task-specific transformation strategies. **(c) Graph convolutional networks framework.** The input of GCNs is the constructed data-rich graphs based on image contents. The GCNs architecture contains input, hidden, and output layers to allow information extraction and inference. **(d) Clinical tasks.** We review a broad range of tasks with clinical relevance that incorporate disease detection, segmentation, and outcome prediction.

2. Methodology of graph convolutional networks

The architecture of graph convolutional networks (GCNs) essentially addresses the cyclic mutual dependencies with weight parameters in each network layer³. The graph convolutional layer updates graph representations by aggregating node information from their neighborhoods. Also, the edge weights and connections will be updated in specified GCNs applications. Conceptually, GCNs could broadly fall into two categories including spectral-based and spatial-based GCNs. First, the spectral-based graph convolutions are defined in the spectral domain based on the graph Fourier transformation³, which can be regarded as an analogy of the signal Fourier transform in 1-D space. Second, the spatial-based graph convolutions are defined in the spatial domain that the aggregations of node representations come from the collective information of neighboring nodes. Also, we discuss important graph pooling modules as downsampling strategies to reduce the size of graph representation¹, which can critically alleviate issues of overfitting, permutation invariance, and computational complexity in the development of graph neural networks. In later sections, we define a graph as $G = (V, E)$, where V is the graph node and E is the edge between nodes. For graph representation learning, we use H to denote the hidden state vector of nodes.

2.1. Spectral graph convolutional networks

Spectral-based graph convolutional networks are derived from the field of graph signal processing, where the spectral-based convolutional operators are defined in the spectral domain¹. Theoretically, a graph signal x will be transformed to the spectral domain by a graph Fourier transform \mathcal{F} before the convolution operation. In this way, the spectral-based graph convolutions can be computed by taking the inverse Fourier transform of the multiplication between two Fourier transformed graph signals⁵. Then the resulting signal is transformed back by the inverse graph Fourier transform \mathcal{F}^{-1} . These transformations are defined as:

$$\mathcal{F}(x) = U^T x, \quad (1)$$

$$\mathcal{F}^{-1}(x) = Ux, \quad (2)$$

U is the matrix of eigenvectors of the normalized graph Laplacian matrix $L = I_N - D^{-\frac{1}{2}}AD^{-\frac{1}{2}}$, where I_N is the normalized identity matrix, D is a node degree matrix and A is the adjacency matrix, which represents the connectivity between every two nodes. L has the property of being real symmetric positive semidefinite. With this property, the normalized Laplacian matrix can be factorized as $L = U\Lambda U^T$, where Λ is a diagonal matrix of all the eigenvalues. According to the graph Fourier transformation, the input graph signal x with a filter $g \in R^n$ is defined as:

$$g \star x = \mathcal{F}^{-1}(\mathcal{F}(g) \odot \mathcal{F}(x)) = U(U^T g \odot U^T x), \quad (3)$$

where \odot denotes the element-wise product, $U^T g$ is a filter in the spectral domain. If we simplify the filter by a learnable diagonal matrix $g_\theta = \text{diag}(U^T g)$, then the spectral graph convolution can be simplified as:

$$g_\theta \star x = U g_\theta U^T x, \quad (4)$$

The majority of spectral-based graph convolutional networks are based on the above definitions, and the design of filter g_θ determines the various performance of individual approaches. Normally, the spectral-based graph convolutional network designs the convolution operation in the Fourier domain by computing the eigen-decomposition of the graph Laplacian². They assume that the filter $g_\theta = \theta_{i,j}^{(k)}$ is a set of learnable parameters and considers graph signals with multiple channels. Due to the eigen-decomposition of the Laplacian matrix, any perturbation to a graph can result in changes of eigenbasis³. The learned filters are domain dependent with a poor graph structure generalization. Also, eigen-decomposition has a high computational complexity that is unfavorable for large-scale data processing. To overcome the limitations, especially the computational complexity, Chebyshev spectral CNN (ChebNet)¹⁴ used K-polynomial filters to achieve a good localization in the vertex domain by integrating the node features within the K-hop neighborhood, i.e. $g_\theta = \sum_{i=0}^k \theta_i T_i \bar{L}$ (4), where $\bar{L} = \frac{2}{\lambda_{max}} L - I_N$, λ_{max} denotes the largest eigenvalue of L . The range of the eigenvalues in \bar{L} is $[-1,1]$. The Chebyshev polynomials are defined recursively as $T_i(x) = 2x T_{i-1}(x) - T_{i-2}(x)$ with $T_0(x) = 1$ and $T_1(x) = x$. The convolution operation can be written as:

$$g_\theta \star x = \sum_{i=0}^k \theta_i T_i \bar{L} x, \quad (5)$$

For a similar purpose of improving computational efficiency, CayleyNet¹⁵ applies the Cayley polynomials that are parametric rational functions to capture narrow frequency bands. The spectral graph convolution operation is defined as:

$$g_\theta \star x = c_0 x + 2\text{Re}\{\sum_{j=1}^r c_j (hL - iI)^{-j} x\}, \quad (6)$$

Where $\text{Re}(\cdot)$ returns the real part of a complex number, c_0 is a real coefficient, c_j is a complex coefficient, i is the imaginary number, and h is the parameter that controls the spectrum of a Cayley filter. ChebNet could be regarded as a special case of CayleyNet via the use of the Chebyshev polynomial approximation to reduce the computational complexity.

A notable variant of ChebNet for further simplifying the computational complexity, which truncates the Chebyshev polynomial to the first-order approximation that the central node only considers its 1-hop neighboring nodes¹⁶. The approach simply filters in (5) with $i=1$ and $\lambda_{max} = 2$ to alleviate the problem of overfitting:

$$g_\theta \star x = \sum_{i=0}^k \theta_i T_i \bar{L} x \approx \theta_0 x + \theta_1 (L - I_N) x = \theta_0 x - \theta_1 D^{-\frac{1}{2}} A D^{-\frac{1}{2}} x, \quad (7)$$

To restrain the number of parameters and avoid overfitting, GCN further assumes that $\theta = \theta_0 = \theta_1$ so that $g_\theta = \theta (I_N + D^{-\frac{1}{2}} A D^{-\frac{1}{2}})$. To solve the exploding or vanishing gradient problem in (7): $I_N + D^{-\frac{1}{2}} A D^{-\frac{1}{2}} \rightarrow \bar{D}^{-\frac{1}{2}} \bar{A} \bar{D}^{-\frac{1}{2}}$, with $\bar{A} = A + I_N$ and $\bar{D}_{ij} = \sum_j A_{ij}$. The propagation layer of GCN is defined as:

$$H = \bar{D}^{-\frac{1}{2}} \bar{A} \bar{D}^{-\frac{1}{2}} X \theta, \quad (8)$$

where $X \in R^{N \times F}$ is the input matrix, $\theta \in R^{N \times F'}$ is the parameter and $H \in R^{N \times F'}$ is the output matrix. F and F' are the dimensions of the input and the output, respectively.

Recent research findings demonstrate the improvement of GCN's feasibility and consistency on graph models. The adaptive graph convolution network (AGCN)¹⁷ could construct and learn a residual graph Laplacian matrix for each sample in the batch through a learnable distance function that takes two nodes' features as inputs. The residual graph Laplacian matrix leads to achieving high-level performance in public graph-structured datasets. In addition, the dual graph convolutional network (DGCN)¹⁸ explores the perspective of augmenting the graph Laplacian as AGCN¹⁷. DGCN jointly considers the local consistency and global consistency on graphs through two convolutional networks. The first convolutional network is the same as (8), while the second network replaces the adjacency matrix with the positive pointwise mutual information (PPMI) matrix.

Spectral-based graph convolutional networks have a solid theoretical foundation derived from graph signals theories. Despite efforts to overcome the computation complexity, the generalization power of spectral-based

GCNs is limited as opposed to the broad usage of spatial-based approaches below. Currently, the spectral-based methods train the filters on the fixed graph structure, making the trained filters unable to apply to a new graph with different structures. However, the graph structures can dramatically vary in both size and connectivity in practical applications¹⁷. The generalization power across different tasks and the high computation complexity become the major hurdles to developing spectral-based graph convolutional networks.

2.2. Spatial graph convolutional networks

The spatial graph convolutional operation essentially focuses on aggregating and updating node representation by propagating node information along edges³. The aggregation strategy can directly improve the generalization power of dealing with different structured graphs by aggregating the information from neighboring nodes and updating the center node representation.

The message-passing neural network (MPNN)¹⁹ represents a general framework of spatial-based GCNs³. The key forward propagation strategy of MPNN is passing the information between nodes through edges directly. As defined in the propagation function below, MPNN runs T steps message-passing iterations so that the information could be propagated between nodes. Notably, GraphSAGE²⁰ is a general inductive framework which generates embeddings by sampling and aggregating features from a node’s local neighborhood. GraphSAGE leverages node feature information to efficiently generate node embeddings for previously unseen data²⁰.

The propagation rule follows:

$$h_{N(v)}^k = \text{AGGREGATE}_k(\{h_u^{k-1}, \forall u \in N(v)\}), \quad (10)$$

$$h_v^k = \sigma(W^k \cdot \text{CONCAT}(h_v^{k-1}, h_{N(v)}^k)), \quad (11)$$

Where AGGREGATE is an aggregator function that could aggregate information from node neighbors. Three types of aggregators are utilized in GraphSAGE, including mean aggregator, LSTM aggregator, and pooling aggregator. W^k is a set of weight matrices that are used to propagate information from different layers. CONCAT is the concatenated operation. Interestingly, GraphSAGE with a mean aggregator can be considered as an inductive version of GCN. To further identify the graph structures that cannot be distinguished by GraphSAGE²⁰, Graph Isomorphism Network (GIN)²¹ is a maximally powerful architecture to distinguish the isomorphism graph. As proved in GIN²¹, the injective aggregation update maps node neighborhoods to different feature vectors so that the isomorphism graph can be distinguished. To achieve the injectivity of the AGGREGATE, sum-pooling is applied in GIN. The AGGREGATE and COMBINE steps are integrated as follows:

$$h_v^{(k)} = \text{MLP}^{(k)}((1 + \epsilon^{(k)}) \cdot h_v^{(k-1)} + \sum_{u \in N(v)} h_u^{(k-1)}), \quad (12)$$

MLP is a multi-layer perceptron that could represent the composition of functions.

The attention mechanism has been increasingly applied in spatial-based GCNs models for various sequence-based approaches^{1,22}. Several key works are attempting to utilize attention mechanisms on graphs. Different from the design of spectral and spatial convolutional operations, the attention-based convolutional operations assign different weights for neighbors to stabilize the learning process and thus alleviate noise effects. A benefit of attention mechanisms is that they allow for dealing with variable-sized inputs, and focusing on the most relevant parts of the input to make decisions²². Graph Attention Network (GAT)²² proposes a computationally efficient graph attentional layer which leverages self-attention and multi-head attention mechanisms. The GAT layer is parallelizable across all nodes in the entire graph while allowing for assigning different importance weights to different (degree) nodes in different size neighborhoods, and does not depend on knowing the entire graph structure. The coefficients computed by the attention mechanism and the propagation of GAT is formulated as:

$$\alpha_{ij} = \frac{\exp(\text{LeakyReLU}(\alpha^T [Wh_i || Wh_j]))}{\sum_{k \in N_i} \exp(\text{LeakyReLU}(\alpha^T [Wh_i || Wh_k]))}, \quad (13)$$

$$h'_i = \sigma(\sum_{k \in N_i} \alpha_{ij} Wh_j), \quad (14)$$

where α and W are weight vectors, and $||$ is the concatenation operation.

Furthermore, GAT leverages multi-head attention²³ to stabilize the learning process of self-attention (14), which can be written as:

$$h'_i = \prod_{k=1}^k (\sum_{j \in N_i} \alpha_{ij}^k Wh_j), \quad (15)$$

$$h'_i = \sigma(\frac{1}{K} \sum_{k=1}^k \sum_{j \in N_i} \alpha_{ij}^k W^k h_j), \quad (16)$$

where α_{ij}^k are normalized attention coefficients computed by the k-th attention mechanism. GAT achieved significant improvement in both transductive tasks and inductive tasks, especially in the inductive task (e.g., protein-protein interaction dataset), GAT improved the micro-averaged F1 scores by 20.5% compared to the best GraphSAGE result.

In summary, spatial-based convolutional graph operations follow a neighborhood aggregation strategy, where we can iteratively update the representation of a node by aggregating representations of its neighbors. After k iterations of aggregation, a node's representation captures the structural information within its k-hop network neighborhood. The rapid development of spatial-based GCNs has displayed their computational efficiency, graph-structure flexibility, and potential generalization across tasks while compared with spectral-based GCNs³. First, spatial-based GCNs tend to be more efficient than spectral-based GCNs because they directly

perform convolutions in the graph domain via node information propagation. Thus spatial-based GCNs do not have to perform eigenvector computation or handle the whole graph computation simultaneously. Second, spatial-based models are flexible to handle multi-sourced graph inputs via the convenient aggregation function³. These graph inputs can be prepared as edge inputs^{24, 25, 26, 27, 28}, directed graphs^{29, 30}, signed graphs³¹, and heterogeneous graphs^{32, 33}. Third, spatial-based models perform graph convolutions locally on each node where network weights can be efficiently generalized across different nodes and graph structures. Therefore, spatial-based models have been shown to achieve superior performance on both transductive (e.g., semi-supervised learning) and inductive (e.g., the traditional supervised learning) tasks with flexibility on graph structures.

2.3. Graph pooling mechanisms

Graph pooling is a key strategy to address the computational challenges derived from graph convolutional operations³⁴. Pooling operations reduce the size of a graph representation while preserving valuable structural information. Typically, graph pooling layers are located after graph convolutional layers and work as a down-sampling strategy. Graph pooling can be categorized into global and hierarchical graph poolings as shown in Fig. 2.

Global pooling operation aggregates the node representations via simple flattening procedures such as summing, averaging, or maxing the node embeddings that are widely used in graph classification tasks³⁴. Further, a global sorting pooling³⁵ sorts the node features in a descending order based on their last feature channel and the k -largest nodes form the updated graph representation of the global sorting pooling layer. Also, global attention pooling³⁶ acts as a soft attention mechanism that decides relevant nodes to the current graph-level task. Such global-wise pooling strategies, also known as readout layers, are often used to generate graph-level representation based on the previous node representations.

Hierarchical pooling operation is designed to refine the node representation by down-sampling strategies and overcome model overfitting. Hierarchical pooling strategies could be further categorized into two types including clustering-based and sorting-based methods. In clustering methods, spectral clustering (SC) offers an efficient means to find strongly-connected communities on a graph. SC can be used in GCNs to implement pooling operations that aggregate nodes especially belonging to the same cluster³⁷. However, the expense of eigendecomposition of the Laplacian and the generalization of SC strategies remain yet to be explicitly addressed. Alternatively, a graph clustering approach³⁷ formulates a continuous relaxation of the normalized min-cut problem and trains GCNs to compute cluster assignments. Spatial-based clustering strategies are proposed to achieve a higher computation efficiency compared with spectral-based clustering strategies. For

example, DIFFPooling³⁸ is a differentiable graph pooling strategy that can generate hierarchical representations of graphs and can be combined with various GCNs architectures in an end-to-end fashion³⁸. The key design of DIFFPooling is to learn a differentiable soft cluster assignment for nodes at each GCNs layer and mapping nodes to a set of clusters, which then forms the coarsened input for the next GCNs layer. In sorting-based methods, they focus on updating the node representation by sorting the nodes and edges depending on their attributes or weights. TopKPooling and SAGPooling shared a similar idea on the node sorting by their attention scores^{39, 40, 41, 42}. These poolings are designed to help select the top-kth nodes to summarize the entire graph for further feature computations. Notably, TopKPooling and SAGPooling can drop the node during model training to improve the computation efficiency and thus overcome the model overfitting. From the graph edge perspective, EdgePooling^{43, 44} is an inspiring example that could drop edges and merge nodes by sorting all edge scores and successively choosing the useful edges with the highest score whose two nodes have not yet been part of a contracted edge.

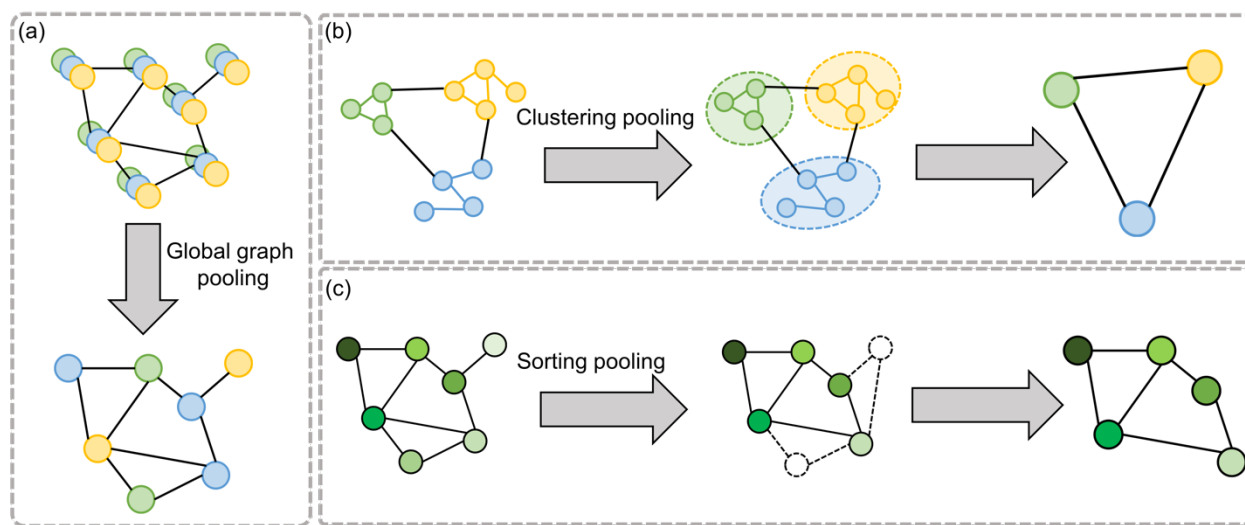


Fig. 2. Graph pooling mechanism. (a) Global graph pooling. The function of global graph pooling is to flatten the node representations to a graph representation. In node representation, each node will include multiple dimensions of node attributes. After utilizing the global graph pooling, the most representative feature will be selected as the node attribute in graph representation. **(b) Clustering graph pooling.** Clustering-based poolings offer an efficient means to find strongly-connected communities on a graph. The nodes in the same clusters are represented by a new cluster node representation. **(c) Sorting graph pooling.** Sorting-based pooling updates the node representation by sorting the nodes attributes or edges weights. Both (b) and (c) are hierarchical pooling operations that refine the node representation to gain model robustness and improve computation efficiency.

2.4. Trade-offs in the design of GCNs architectures

To optimize the performance of graph network models, there are multiple trade-offs between the network architecture and the corresponding model performance. The ability of information collection and the strategy of effective aggregation are crucial factors for measuring the performance of GCNs models. Intuitively, a deeper architecture corresponds to a larger receptive field, which can collect more auxiliary information towards enhanced performance of GCNs. However, the performance might decrease when layers go deeper to evolve larger receptive fields in real applications²⁵. Such performance deterioration could be attributed to the over-smoothing of node representation with an increased architecture depth. In other words, the repeated and mixed message aggregation can lead to node representations of inter-classes indistinguishable⁴⁵. It is commonly seen that the over-smoothing issue always occurs in the nodes with a dense connection with other nodes (e.g., the core of the graph) that could rapidly aggregate information in the entire graph. In contrast, the node in the tree part (e.g., leaves of the tree) could only include a very small fraction of information of all nodes with a small number of GCNs layers. To improve the GCNs model performance, it is necessary to overcome the graph over-smoothing phenomena and achieve informative node representation. For example, the study⁴⁶ implemented a co-training and self-training scheme with a smoothness regularizer term and adaptive edge optimization⁴⁵ to alleviate the over-smoothing problem. Co-training a GCN with the random walk model can explore the global graph topology. Further, self-training a GCN could exploit feature extraction capability to overcome its localized limitation. Informative node representation via the jumping knowledge network (JK-Net)⁴⁷ tends to demonstrate compelling performance on graph computing efficiency and alleviate overfitting. Notably, the idea of layer-aggregation across layers helps select the most informative nodes and reduce the overfitting issue, and the LSTM-attention could further identify the useful neighborhood ranges. Inspired by the architecture of JK-Net, Deep adaptive graph neural network (DAGCNs)²⁵ developed an adaptive score calculation scheme for each layer, which could balance the information from both local and global neighborhoods for each node. Both JK-Net and DAGCNs aim to find a trade-off between accuracy performance and the size of receptive fields by adaptively adjusting the information from local and global neighborhoods. For the design of network architecture, we expect additional efforts to overcome the over-fitting issues while keeping a flexible architecture to explore more meaningful information in the context of disease detection and diagnosis.

3. Development of GCNs in medical imaging

3.1 Radiological image analysis

Over the past decades, multi-modality radiological images have been routinely utilized in abnormality segmentation^{48, 49}, detection^{50, 51}, and patient outcome classification^{52, 53}. In this section, we discuss the growing body of GCNs studies applied to radiological analysis^{54, 55, 56}, including magnetic resonance imaging (MRI), Computed Tomography (CT), and X-ray imaging. The combination of GCNs and radiological imaging promises

to reflect the interaction among tissue regions and provide an intuitive means to fuse the morphological and topological-structured features among key image regions to advance modeling, interpretation, and outcome prediction. We here discuss the representative neuroimaging research and other related studies to highlight the usefulness of GCNs across different radiological imaging modalities and clinical tasks.

3.1.1 Neuroimaging

In neuroimaging, multi-modality MRI is a useful diagnostic technique by providing high-quality three-dimensional (3D) images of brain structures with detailed structural information⁵⁷. Conceptually, multi-modality MRI data can be categorized into functional MRI (fMRI), structural MRI (sMRI), and diffusion MRI (DMRI). The fMRI measures brain activity and detects the changes in blood oxygenation and blood flow in response to neural activity⁵⁸. The sMRI translates the local differences in water content into different shades of gray that serve to outline the shapes and sizes of the brain's various subregions⁵⁹. The DMRI is a magnetic resonance imaging technique in which the contrast mechanism is determined by the microscopic mobility of water molecules⁶⁰. All these imaging modalities provide vital diagnostic support for neurological disease analysis because they can capture anatomical, structural, and diagnosis-informative features in neurology. Therefore, the overarching goal is to develop useful graph network models to define, explore, and interpret interactions of brain neurons and tissues. The detailed process of utilizing GCNs in the neuro-imaging analysis is illustrated in Fig. 3.

To analyze the complex brain region connectivity and interaction, a brain graph representation can intuitively portray human brain organization, neurological disorders, and associated clinical diagnosis. Conventionally, the human brain could be modeled into a brain biological network containing nodes (e.g., region of interests) and edges among brain network nodes. The edges could be determined by brain signals or the real fiber connection. Yet these biologically-defined networks are often unable to faithfully capture neurological disorders and outcomes of patients⁶¹. To overcome this challenge, it is encouraged to leverage informative image-based features to considerably enrich graph node attributes. Comprehensive graph representation can integrate multiple types of information (e.g., image features, human brain signals, and clinical data) to greatly expand the knowledge base of brain dynamics and potentially provide auxiliary clinical diagnosis assistance. The use of GCNs here can be helpful to augment the architecture of human brain networks and has achieved remarkable progress in explaining the functional abnormality from the network mechanism⁶². In particular, GCNs are able to consider the functional or structural relations among brain regions together with image-based features that are beyond the scope of the conventional CNN-based methods^{63, 64, 65}. The CNN-based model is merely viewed as a feature extractor for disease representation without consideration of structure information of the brain. For example, the deep 3-D convolutional neural network architecture was not unable to capture underlying structure information for Alzheimer's disease classification using brain MRI scans⁶¹. By contrast,

the convergence of GCNs methods and MRI provide an alternative means to characterize the architecture of human brain networks and has achieved outstanding progress in brain abnormality explanation⁶².

The graph representations can be divided into functional and structural brain connectivity graphs based on the definitions of the graph components. First, graph nodes are regions of interest (ROI) as defined in MRI. ROI definition is commonly done through the anatomical parcellation of the Montreal neurological institute (MNI) using sMRI and fMRI data^{66, 67, 68}. Second, graph edges are determined by the physical connectivity (e.g., the fiber tracts) of nodes in structural brain networks while calculated from the signal series analysis in functional brain networks. We therefore discuss insights of functional and structural brain connectivity graph developments below.

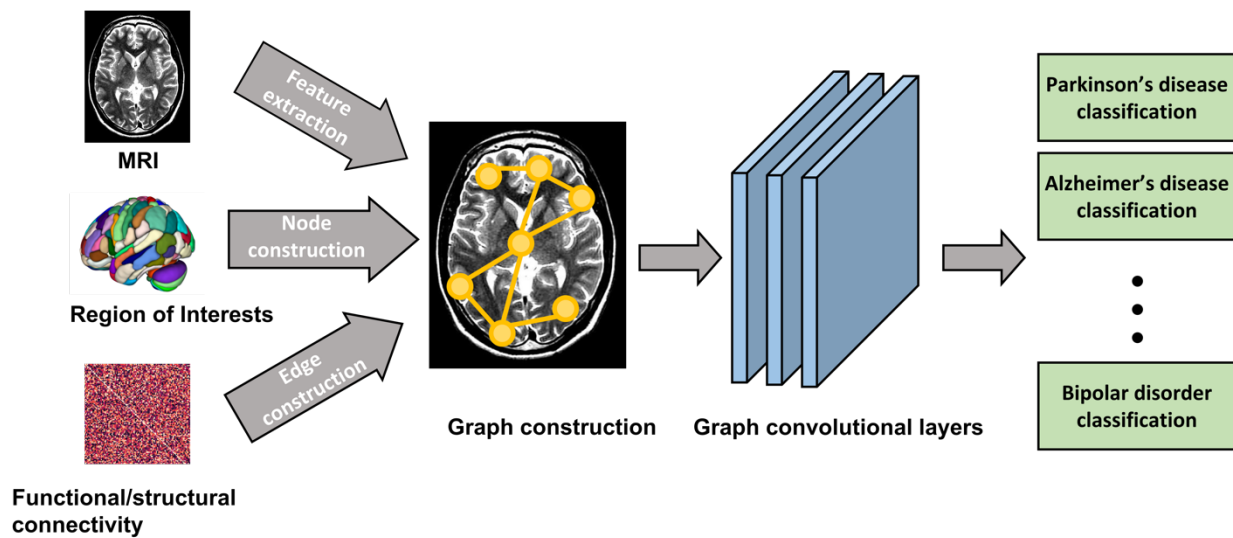


Fig. 3 The framework of developing GCNs in neuro-imaging analysis. Multi-modality MRIs are firstly converted into graph structure which is determined by the region of interest in terms of real human brain signals or fiber connectivity (e.g., node and edge definitions). Through graph-level model development and inference, we highlight numerous image-based analysis and diagnosis of diseases in neurology.

The human brain functional connectivity denotes the functional relations between specific human brain areas and functional brain graphs can represent estimates of interactions among time series of neuronal activity⁶². In functional brain networks, the nodes are defined as ROIs while the node attributes could be hand-crafted features or correlation measurements between nodes. The edges are created through the node correlations between different regions. For example, the GCNs framework achieved high-level performance in classifying Autism spectrum disorders (ASD) and healthy controls (HC) using task-functional magnetic resonance imaging (task-fMRI) through the appropriate ROI definition⁶⁹. The brain is parcellated into multiple ROIs based on its T1 structural MRI and the edges among ROIs are determined by calculating the node correlation. Concretely, the nodes (e.g., ROIs) attributes were handcraft features and the edge attributes are calculated by the Pearson

correlation and partial correlation which is calculated between the centers of the two ROIs. Notably, their model consists of a message-passing neural network (MPNN)¹⁹ as convolutional layers that is invariant to graph symmetries⁶⁹. Furthermore, Top-k poolings³⁹ is able to downsample the node to achieve a higher computation efficiency while preserving a meaningful graph delineation. Inspired by metric learning, a siamese graph convolutional neural network (s-GCN) is proposed for the ASD and HC classification purpose⁵⁴, where samples were collected from Autism Brain Imaging Data Exchange (ABIDE)⁷⁰ database and UK Biobank⁷¹. The graph metric learning method essentially utilized GCN layer¹⁶ in a siamese network⁷². Two types of graph construction methods are designed as the input of the model, such as spatial and functional graphs which determine nodes by ROIs. The spatial graphs construct a KNN graph based on spatial coordinates of the ROI. Different from spatial graphs, the functional graph constructs a KNN graph using the correlation distance between all ROI pairs. The functional graph is more meaningful to reflect the average functional connection strength between pairs of brain regions within a population. Both of these two graph construction strategies use Pearson's correlation to obtain a functional connectivity matrix and define the node attributes. The inputs for s-GCN are two same structure spatial or functional graphs with different signals (e.g., rows or columns of functional matrix).

The human brain's structural connectivity in vivo can be captured by structural and diffusion MRI^{73, 74}, and structural brain graphs could represent anatomical wiring diagrams⁶². Similar to the definition of nodes in functional connectivity networks, the nodes in structural connectivity networks are defined as a region of interests (ROIs). Clinically, the structural brain connectivity represents the structural associations of altered neuronal elements, including both the morphometric alternation and accurate anatomical connectivity as seen in imaging. In the complex brain networks, structural brain connectivity assesses to white amount projections bond cortical and subcortical regions⁷⁵. The edges indicate the actual neural fiber connections between different brain regions. For example, a stack architecture design of combining a heterogeneous GCN model⁵⁵ with an efficient adaptive pooling scheme³⁸ is able to predict the clinical score of Parkinson's disease (PD) and HC using diffusion-weighted MRI (DWI) on Parkinson Progression Marker Initiative (PPMI)⁷⁶. This approach shows great potential for analyzing multi-modality brain network problems via an efficient graph construction. To construct the graph structure from DWI, firstly, nodes are defined by the ROIs in the brain, which are parceled from the brain based on its T1 weighted MRI. Second, three whole-brain probabilistic tractography algorithms are able to determine different brain structural graphs using three whole-brain probabilistic tractography algorithms. The node attributes corresponding to rows in the human brain network are defined as features. Novelty, a framework is developed to explore graph structure in the q-space by representing DMRI data and utilizing graph convolutional neural networks to estimate tissue microstructure⁷⁷. This approach is capable of not only reducing the data acquisition time but also accelerating the estimation procedure of tissue microstructure. The nodes of the weighted graphs are sets of points on a manifold. Also, the adjacency weights are defined between two nodes using Gaussian kernels, accounting for differences in gradient directions and diffusion weightings. The q-space signal measurements are represented by using the constructed graph that

encodes the geometric structure of q-space sampling points. A residual ChebNet¹⁴ can learn the mapping between sparsely sampled q-space data and high-quality estimates of microstructure indices.

Beyond single-modality MRI analysis, multi-modality data analysis emerged as active research areas for GCNs modeling. The data fusion could occur in different image data or between imaging and non-imaging data. Multi-modality MRI data analysis is able to deepen our understanding of disease diagnosis from different data aspects. In neuroimaging, the structural connectivity in sMRI reflects the anatomical pathways of white matter tracts connecting different regions, whereas the functional connectivity in fMRI encodes the correlation between the activity of brain regions. A unique advantage of multi-modality MRI data analysis is that they have incorporated complementary information from different modalities simultaneously. For instance, the study⁷⁸ introduced an edge-weighted graph attention network (EGAT)²² with a diffPooling³⁸ to classify Bipolar disorder (BP) and HC from sMRI and fMRI in cerebral cortex analysis. To construct the brain networks, the node attributes contain seven anatomical features and four functional connectivity statistical features derived from either sMRI or fMRI. The edges are determined by the densely connected graph without dismissing the weak connectivity. The edge weight is determined by Pearson's correlation-induced similarity between regions. Also, the framework of Siamese community-preserving graph convolutional network (SCP-GCN)⁷⁹ is able to learn the structural and functional joint embedding of brain networks on two public datasets (i.e., Bipolar and HIV dataset⁷⁹). Especially, siamese architecture can exploit pairwise similarity learning of brain networks to guide the learning process to alleviate the data scarcity problem⁷⁹. Ninety cerebral regions are selected as nodes for both structural (e.g., Diffusion Tensor Image (DTI)) and functional (e.g., fMRI) networks, and the node attribute is determined by the functional connectivity between nodes corresponding to fMRI. The edge connectivity is determined by the DTI via a series of preprocessing (distortion correction, noise filtering, repetitive sampling from the distributions of principal diffusion directions for each voxel). To preserve the community property of brain networks, the design of a community loss presents its usefulness to minimize the intra-community loss and maximize the intercommunity loss. Furthermore, GCNs allow the integration between MRI and non-imaging data for analyzing complex disease patterns. For example, an Edge-Variational GCN (EV-GCN)¹¹ could automatically integrate imaging data (e.g. fMRI data) with non-imaging data (e.g. age, gender and diagnostic words) in populations for uncertainty-aware disease prediction. They constructed weighted graphs via an edge-variational population graph modeling strategy. In the weighted graphs, the graph nodes are ROIs and the node attributes are features extracted from histology and fMRI images. It is particularly notable that the weight of the edge is achieved by a learnable function of their non-imaging measurements. The proposed Monte-Carlo edge dropout (MCED) randomly drops a fraction of edges in the constructed graphs to reduce overfitting and increase the graph sparsity.

3.1.2 X-ray and CT imaging

Extensive studies have also utilized GCNs in X-ray and Computed Tomography (CT) images for disease analysis^{56, 80, 81}. Different from MRI data, CT images are able to reflect the vessel skeleton information that could assist a variety of clinical tasks. For example, chest CT scans can assist with arteries-veins separations that are of great clinical relevance for chest abnormality detection⁸⁰. The graph was constructed of the voxels on the skeletons resulting in a vertex set and their connections in an adjacency matrix. The skeletons are extracted from chest CT scans by vessel segmentation and skeletonization. In this study⁸⁰, GCN layers can extract and learn connectivity information. The one-degree (direct) neighbors were considered and the vertices attributes were extracted by CNN model to consider the local image information. In addition, the study⁵⁶ proposed an end-to-end hybrid network to train a CNN and GAT network to leverage both advanced feature learning and inter-class feature representations on Chest-Xray 14 dataset⁸². To utilize the image sequencing information, they determine each image from the same patient as a vertice of a graph and the extracted features are the attributes of vertices. Furthermore, they leverage non-imaging meta-data, such as clinical information, to construct edges between the vertices. After constructing the graph and updating the graph representation with GAT, they combine the CNN extracted features with graph representation by skip-connectivity to achieve hybrid representation. The motivation of generating hybrid representation is to improve the distinction between samples. Due to the pandemic of COVID-19, GCNs have also been utilized in disease detection. GraphCovidNet⁸¹ utilized GIN for COVID-19 detection on both CT and X-ray images. The graph is used to depict the outline of an object (e.g., organ) in the image. First, they applied edge detection to determine the edge outline. Then, the graph nodes are defined by the pixel having a grayscale intensity value greater than or equal to 128, which implies nodes reside only on the prominent edges of the edge image. The node attribute consists of the grayscale intensity of the corresponding pixel. An edge exists between the two nodes which represent neighboring pixels in the original image.

Table1 summarizes a variety of graph construction methods and GCNs application in radiologic image analysis. Compared to conventional methods, GCNs methods for the analysis of brain networks have the possibility of combining image-based features with the conventional brain networks.

Table 1. Summary of GCNs in radiologic image analysis

Method	Category	Input	Graph Construction		
			Edge	Node	Node/Edge Attributes
69	Single-modality	Task-fMRI	Region-to-region correlations	ROIs	Node: hand-craft features

			(threshold edges under 95% partial correlation)		Edge: values of Pearson correlation and partial correlation between nodes.
54	Single-modality	fMRI	Spatial graph: a KNN graph based on spatial coordinates of the ROI.	ROIs	Rows/column of the functional connectivity matrix
			Functional graph: a KNN graph using the correlation distance between all ROI pairs.		
55	Single-modality	DWI	whole-brain probabilistic tractography algorithm	ROIs	Rows/column of the connectivity matrix
77	Single-modality	DMRI	Constructing the edge between two nodes when edge weights are larger than 0.	Points on manifold	In q-space using two Gaussian kernels, accounting for differences in gradient directions and diffusion weighting
80	Single-modality	CT	The voxels on the skeletons	The connectivity of voxels	Extracted by CNN model
81	Single-modality	CT And X-ray	The neighborhood relationship between pixels	Pixel	Grayscale intensity of the pixel
78	Multi-modality	fMRI and sMRI	Densely connected graph	ROIs	Node: seven anatomical features and four functional connectivity statistic features.
					Edge: the Pearson correlation-induced similarity.

79	Multi-modality	fMRI and DTI	Region-to-region correlations	ROIs	Rows/column of connectivity matrix
11	Multi-modality	fMRI and clinical data	Connectivity the vertices	ROIs	Node: image features
					Edge: non-image information
56	Multi-modality	X-ray and meta-data	Non-image meta-data	Image	Extracted features by CNN.

3.2. Histopathological image analysis

The growth of digitalized histopathological images presents a valuable resource to support rapid and accurate clinical decision making. The high-resolution whole slide image (WSI) contains rich tissue characteristics including patterns of cell nuclei, glands, and lymphocytes^{83, 84}. Extensive pathological characteristics of tissue and cell interactions can be evidently observed that are not available in other clinical image data. For instance, lymphocytic infiltration of cancer status can be deduced only from histopathology imagery⁸⁵. These pathological patterns can be used to build the biological graph networks that can inform disease status and thus discern predictive imaging biomarkers. Overall, we recognize that GCNs analysis is uniquely positioned to address key issues of histopathological applications, including data annotation, tissue connections, global-local information diagnostic fusion, and model prediction performance in challenging settings.

Developments of GCNs have brought remarkable advances into computational histopathology including label efficiency and multi-scale context representation. First, graph structure provides a reasonable choice to represent the entire slide in terms of tissue content connectivity. Such entire-slide graph representation can avoid fine-grained patch-wise label annotation. Since we know that patch-level labeling is highly time-intensive, even impossible, to include all ranges of tumor patches annotated by human experts. Second, graph structural representation can capture multi-scale contexts considering both global and local image-wise features towards enhanced prediction of disease outcomes. Third, graph structural representation builds upon the interaction among spatially-separated tiles that enables a more flexible and comprehensive receptive field. Such advances are analogous to the workflow of human experts that we consider tumor environment, tissue contents, and their interactions, rather than single tumor tiles, to diagnose tissue status of patients.

Because the high-resolution histopathological image does not present a natural form of graph structure, efficient graph representation becomes a vital factor for model development and optimization. Current graph construction in histopathology can be broadly categorized into patch-based and cell-based methods. First, patch-based graph construction methods aim to enable information extraction by considering the entire micro-environment (e.g., the cells and tissues), where comprehensive tissue micro-environment and cell dynamics can be captured. In these patch-based methods, graph nodes are defined as the selected patches determined by ROIs in the histopathological image. The associated node attributes can be extracted by standard feature extractors (e.g., ResNet18 or VGG16). Graph edges are defined as the connectivity between nodes, which is determined by the feature or coordinate distance between two nodes. A smaller distance means a higher probability of connectivity. The connectivity between nodes could determine an adjacency matrix to represent the entire topological structure of the graph. Although the definition of primitive graph components (e.g., node and edge) are conceptually similar, most patch-based graph construction methods have different settings for node attributes and edge construction. As opposed to the patch-based graphs, cell-based graph methods emphasize the possible biological significance derived from histopathology. Cell-based graph construction methods aim to model the relationship between different cells and the micro-environment (e.g., tissues or vessels) utilizing graph-based features⁸⁶. In a cell graph, the detected and segmented nuclei or cell clusters are considered as nodes. The node attribute is defined as the combination of image-wised features, such as features extracted by CNN models, and the hand-crafted feature, such as the number or the size of nuclei, the average RGB value of nucleus, gray level co-occurrence matrix features, VGG19 features, and the number of neighbors of a nucleus⁸⁷. According to the assumption that adjacent cells are more likely to interact⁸⁶, the edge between the nodes can be determined via Delaunay triangulation⁸⁸ or the K-nearest-neighbour method⁸⁹, which could evaluate whether two cells (nodes) belong to the same cluster. The cells in the same cluster are more likely to have an edge between them. Despite a good performance on clinical classification tasks, these approaches cannot work well in capturing the diagnostic and prognostic information from the surrounding micro-environments (e.g., tissues and vessels). Meanwhile, constructing cell-centered graphs highly depends on cell detection accuracy. It is notable that constructing a cell-based graph and subsequent graph computing need an excessive computational complexity. The process of utilizing GCNs in histopathological image analysis is shown in Fig. 4. We outline several areas of clinical interest for GCNs in histopathology below.

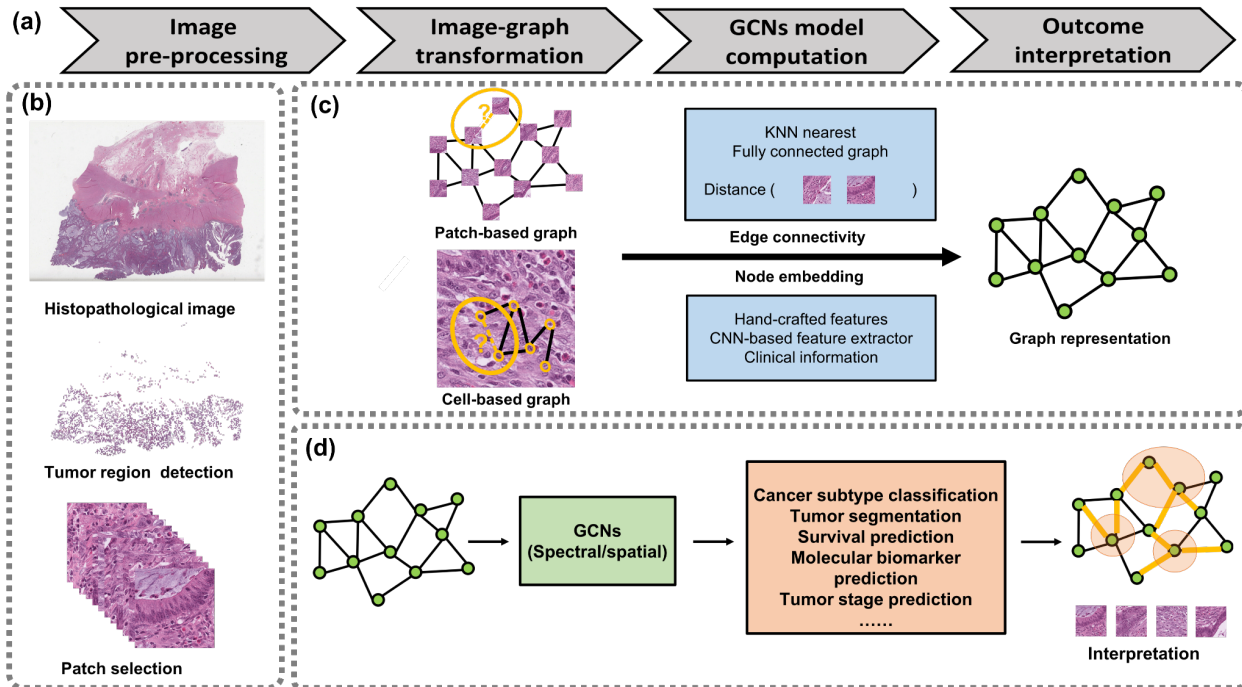


Fig 4. The illustration of the computational framework of GCNs in histopathological imagery. (a) Overall steps of image-based graph convolutional network framework. (b) Image preprocessing. The high-resolution images are normally split into manageable small-sized tumor tiles. We primarily focus on tumor tile preprocessing and analysis for GCN development. **(c) Image-based graph transformation.** The transformation between image and graph-structured data is vital according to different tasks. Both patch-based and cell-based graphs can be established for downstream tasks. **(d) GCNs computation and outcome interpretation.** The inputs of GCNs are the constructed image-based graphs. The outcome interpretation of GCNs includes both node- and edge-wise findings to enable a multi-dimensional interpretation of outcomes.

3.2.1 Tumor segmentation

Accurate tumor segmentation in histopathology is designed to assist pathologists for improving workflow efficiency of clinical diagnosis⁷. Graph-based segmentation approaches can incorporate both local and global inter-tissue-region relations to build contextualized segmentation and thus improve the overall performance. For example, *SEGGINI* performs semantic segmentation of images by constructing tissue-graph representation and performing weakly-supervised segmentation via node classification by using weak multiplex annotations, i.e., inexact and incomplete annotations, in prostate cancer⁷. In this study, they defined graph nodes by superpixels merging based on channel-wise color similarity of superpixels at higher magnification. The node attribute is determined by the spatial and morphological features of the merged node (e.g., the merged superpixel). The spatial feature is computed by normalizing superpixel centroids by the image size and the morphological feature is extracted by a pre-trained MobileNetV2⁹⁰. They defined the edges by constructing a region adjacency graph (RAG)⁹¹ from the spatial connectivity of superpixels. The local and global connection of

tissue details creates an alternative avenue for pixel-level segmentation evaluation that draws a contrast to other conventional convolutional-based tumor segmentation approaches^{92, 93, 94}.

3.2.2 Cancer tissue classification

Cancer subtype classification is crucial in clinical image analysis that can impact patient stratification, outcome assessment, and treatment development^{6, 95}. GCNs have been extensively studied in cancer subtype classification due to their unique ability to explore the relational features among tissue sub-regions (e.g., patches or cells). Patch-based graph construction approaches are intuitive to build a bridge between image features and graph structure. Conceptually, patches are defined as nodes and node attributes are extracted patch features, including CNN-based extracted and hand-crafted features. The edges are typically determined by the Euclidean distance of nodes. For example, the combination of ChebNet¹⁴ and GraphSage²⁰ presents its usefulness for classifying lung cancer subtypes in histopathological images⁶ via patch selection. All patches in the tissue region are grouped into multiple classes, and a portion of all clustered patches (e.g., 10%) are randomly selected within each class. Also, a simplified graph construction process⁶ can be useful to leverage all patch information. The global context among patches is considered while using a fully connected graph to represent the connection among nodes. Global pooling layers (e.g., global attention, max, and sum poolings) are able to generate graph representations for analyzing cancer classification. In particular, global attention pooling³⁶ provides strong interpretability to determine which nodes are relevant to the current graph-level classification tasks. In colorectal cancer histopathology, ChebNet¹⁴ framework shows its predictive power in lymph node metastasis (LNM) prediction⁹⁵. Interestingly, a combination model of a variational autoencoder and generative adversarial network (VAE-GAN)⁹⁶ is utilized to train as a feature extractor to decode the latent representations closer to their original data space.

As opposed to patch-based approaches, cell-based graph construction is under a key assumption that cell-cell interactions are the most salient points of information⁹⁷. A common example is to define the detected nuclei as nodes⁸⁷ and while the overall node attributes are aggregated by concatenating multiple types of features (e.g., average RGB value, gray level co-occurrence matrix features, VGG19 features, and the number of neighbors of a nucleus). The graph edge is determined by thresholding the Euclidean distance between nodes. In addition, the cell graph convolutional network⁸⁶ presents a generalized framework for grading colorectal cancer histopathological images based on the combination of GraphSage⁹⁷, JK-Net⁴⁷, and Diffpooling³⁸. The node attributes are defined by 16 hand-craft features incorporating shape, texture, and color attributes, and 17 nuclear descriptors. The edge between two nuclei is determined by a fixed distance while the maximum degree of each node is set to k corresponding to its k -nearest neighbors. Sharing a similar cell-graph construction strategy and graph component definition with⁸⁶, a GIN-based²¹ framework is designed for breast cancer subtype classification⁹⁸. In addition, the clinical interpretation is provided by a cell-graph explainer that is inspired by a previous graph explainer⁹⁹, a post-hoc interpretability method based on graph pruning

optimization. The cell-graph explainer is able to prune the redundant graph components, such as the nodes that could not provide enough information in the decision making, and define the resulting subgraph as the explanation. Another cell graph application of cancer classification¹⁰⁰ is built on top of robust spatial filtering (RSF)³², where RSF combined with attention mechanisms to rank the graph vertices in their relative order of importance, providing visualizable results on breast cancer and prostate cancer classification.

To leverage the advantages of patch- and cell-based graphs simultaneously, the model integration can provide additional auxiliary benefits by capturing detailed nuclei and micro-environment tissue information. A hierarchical cell-to-tissue graph neural network (HACT-Net)¹⁰¹ is an example to consist of a low-level cell-based graph (e.g., cell-graph), a high-level patch-based graph (e.g., tissue-graph), and a hierarchical-cell-to-tissue representation for breast carcinoma subtype classification. For the cell-based graph, they defined nuclei as graph nodes that are detected by the pre-trained Hover-Net^{50, 102, 103}. For the patch-based graph, they determined graph nodes and their attributes by creating non-overlapping homogeneous superpixels and their features. The edges are constructed by a region adjacency graph⁹¹ using the spatial centroids of the super-pixels. Overall, such a joint analysis across histopathological scales leads to enhanced performance for cancer subtype classification.

Cancer staging classification is also of clinical significance that comprises tumor tissue and nodal (e.g., tumor and lymph nodes) staging⁹⁷. Patch-based graph construction strategies are commonly used in tumor staging classification in terms of graph attention⁸. Also, graph topological feature extraction is useful in colon cancer tumor stage prediction with well interpretation⁹⁷. In particular, they utilized the Mapper¹⁰⁴ to project high-dimensional graph representation to a lower-dimensional space, summarizing higher-order architectural relationships between patch-level histological information to provide more favorable interpretations for histopathologists.

3.2.3 Survival prediction

Survival analysis is a long-standing clinical task to determine the prognostic likelihood of patients^{95, 105}. Both cell- and patch-based approaches can be considered to capture survival sensitive information of patients. For instance, the graph convolutional neural network with attention learning has shown to achieve a good performance on the survival prediction in colorectal cancer¹⁰⁶. Tumor tiles are defined as nodes and node attributes are extracted by the VGG16. Graph edges are constructed by thresholding the Euclidean distances between node attributes. After constructing the graph, they used the ChebNet¹⁴ framework for survival analysis on the histopathological images. In addition, cell-based and patch-based graphs can be further unified to allow a trade-off between efficiency and granularity¹⁰⁷. They used GAT for prostate cancer survival prediction using WSIs. Notably, a self-supervised learning method is proposed to pretrain the model, yielding improved performance over trained-from-scratch counterparts. For cell-based graphs, they use a Mask R-CNN¹⁰⁸ for

nuclei segmentation and define an eight-pixel width of the ring-like neighborhood region around each nucleus as its cytoplasm area. The nuclear morphometry features and visual texture features (intensity, gradient, and Haralick features) have made substantial contributions for both nuclear and cytoplasm region representations respectively. Despite these advances, uncertainty remains for exploring definitive roles of cell-level and patch-level characteristics with regard to overall survival likelihood of patients.

3.2.4 Molecular biomarker prediction

Image-based molecular biomarker prediction is promising to deepen our understanding of cancer biology across data modalities. Enormous efforts are gaining momentum to explore multiple image-to-genome associations in cancer research^{109, 110, 111}. The feature-enhanced graph network (FENet)¹² leverages histopathological-based graph structure to predict key molecular outcomes in colon cancer. Through the spatial measurement of tumor patches, the image-to-graph transformation illustrates its unique value in predicting key genetic mutations. In particular, the use of GIN²¹ layer and jumping knowledge structure are useful to aggregate and update the patch embedding information. Alternatively, the cell-based construction method is considerable for cancer biomarker prediction¹¹². HoverNet¹⁰³ is a popular choice for nuclei segmentation to support cell graph construction. Next, the agglomerative clustering¹¹³ is utilized to group spatially neighboring nuclei into clusters. These clusters can be defined as graph nodes and the node attribute is determined by the standard deviation of nuclei sizes. Meanwhile the edges are constructed by using Delauney triangulation based on the geometric coordinates of cluster centers with a maximum distance connectivity threshold. Both cell- and patch-based approaches contribute to the integration of histopathology and genome as more biological data become accessible. We recognize that graph-based models can offer an efficient means to measure the cross-modality differences, which requires careful inputs on graph construction, model layer architectures, proper design of feature extraction for achieving improved performance of molecular outcome prediction.

Overall, Table 2 summarizes the category, type of tasks, and the graph-structure construction strategies. In this chapter, we have discussed novel perspectives for computational histopathological image analysis. In particular, GCNs-based methods provide a novel perspective to consider tumor heterogeneity in histopathological image analysis. Despite multiple challenges, the evolving capacity of current graph construction strategies (edge, node, and node attributes) makes it possible to address a variety of clinical tasks using histopathological images.

Table 2. Summary of GCNs in histopathological image analysis

Method	Category	Tasks	Graph Construction		
			Edge	Node	Node Attribute
7	Patch-based	Segmentation	Region adjacency graph	Superpixel	1. Normalizing superpixel centroids by image size 2. Extracted by a pre-trained MobileNetV2
95	Patch-based	LNM prediction	Euclidean distance of node attributes	Image Patch	Extracted features of images patch and closer the feature space to the original one by VAE-GAN
106	Patch-based	Survival prediction	Euclidean distances between node attributes.	Image Patch	Extracted features of images patch by VGG16
6	Patch-based	Cancer Type/subtype classification	Fully connected graph attribute	Image Patch	Extracted features of images patch by DenseNet
12	Patch-based	Biomarker Prediction	Thresholding the Euclidean distance between node coordinates	Image Patch	Extracted features of images patch by ResNet18
97	Patch-based	Tumor Stage Prediction	The relationship between nodes	Image Patch	Extracted features of images patch
8	Patch-based	Tumour Node Metastasis (TNM) staging Prediction	The connectivity between nodes and their KNN neighbors in a fixed threshold	Image Patch	Texture feature extraction.

87	Cell-based	Cancer Type/subtype classification	Thresholding the Euclidean distance between nuclei	Nuclei	Concatenating multiple types of features, including average RGB value, gray level co-occurrence matrix features, VGG19 features, and the number of neighbors of a nucleus.
86	Cell-based	Cancer Type/subtype classification	The connectivity between nodes and their KNN neighbors	Nuclei	16 hand-craft features and 17 nuclear descriptors
98	Cell-based	Cancer Type/subtype classification	Threshold the kNN graph by removing edges that are longer than a specified distance	Nuclei	16 hand-crafted features
100	Cell-based	Cancer Type/subtype classification	The Euclidean distance between nuclei	Nuclei	Concatenating edge and vertex features of a node
107	Patch-based	Survival prediction	The connectivity between nodes and their KNN neighbors (K=5)	patch	Image features and cell-based graph representation
	cell-based		The connectivity between nodes and its KNN neighbors (K =3)	Nuclei	Nuclear morphometry features and imaging features (including intensity, gradient and Haralick features)
112	Cell-based	Biomarker prediction	Delauney triangulation between cluster center with a maximum distance	The geometric center of nuclei	The count of the six nuclei types and the standard deviation of nuclear sizes

			threshold	cluster	
101	Patch-based	Cancer subtype classification	Region adjacency graph	Superpixel	Features of superpixels
	Cell-based		The connectivity between nodes and their KNN neighbors	Nuclei	Hand-craft features

4. Other image-based applications

GCNs have demonstrated their analytical ability in alternative medical image disciplines to facilitate structural analysis of disease diagnosis (e.g., eye disease and skin lesion). For instance, GCNs have been studied in dermatology and eye-related diseases, involving retinal, fundus, and fluorescein angiography (FA) images^{105,114,115,116}. GCNs could also be utilized in immunohistochemistry (mIHC) images for survival analysis¹⁰⁵. Similar to radiological and histopathological images, patch-based graph construction strategies are widely used in the above image domains. GCNs have shown to be valuable to learn the vessel shape structures and local appearance for vessel segmentation in retinal images¹¹⁴. Also, GCNs were applied to the artery and vein classification by using both fundus images and corresponding fluorescein angiography (FA) images¹¹⁵. With a designed graph U-Nets architecture⁴⁰, the high-level connectivity of vascular structures can be learned from node clustering in the node pooling layers. Furthermore, GCNs show their power in differential diagnosis of skin conditions using clinical images. This problem is formulated as a multi-label classification task over 80 conditions when only incomplete image labels are available¹¹⁶. The label incompleteness is addressed by combining a classification network with a graph convolutional network that characterizes label co-occurrence¹¹⁶. Each clinical image is defined as a graph node and the connectivity between two nodes is determined by domain knowledge of skin condition by board-certified dermatologists. It is noteworthy that edge connection is made by inputs from human experts that two dermatologists provide overlapped differential diagnoses groups, and connect an edge when two labels appear in at least one differential group by both dermatologists. In addition, a cell-based graph analysis¹⁰⁵ combines multiple types of GCNs with graph poolings, including GIN^{20, 21}, GraphSage²¹, and GCN¹⁶ for survival prediction of gastric cancer using immunohistochemistry (mIHC) images. The graph nodes are determined by six antibodies of PanCK, CD8, CD68, CD163, Foxp3, and PD-L1, which were used as annotation indicators for six different types of cells. The node attributes are determined by cell locations, types, and morphological features. The edges are constructed by the maximum effective distance between immune and tumor cells, which is equivalent to 40 pixels in the magnification of this study.

Table 3. Summary of GCNs in other image analysis

Method	Image type	Tasks	Graph Construction		
			Edge	Node	Node/edge Attribute
105	Immunohistochemistry (mIHC) images	Survival prediction	Euclidean distances between nodes.	Cell	Node: the cell locations, optical features of stained cells, and morphology features
					Edge: $\frac{40}{\text{distance between cells}}$ (set to 0 while no interaction between nodes)
114	Retinal image	Vessel Segmentation	Geodesic distance between nodes (smaller than a fixed threshold)	Pixels with maximum vessel probability	Extracted by CNN.
115	Fundus images and corresponding fluorescein angiography (FA) images	The artery and vein classification	Edges are constructed with existing vessel pixels within an $N \times N$ local patch.	Vessel pixels with in $N \times N$ local patches	Extracted by graph U-nets.
116	Skin clinical images	Skin condition classification	Connected an edge when two labels appear in at least one differential group by both dermatologists.	Image	Node: Extracted by CNN
					Edge: $\frac{C(i,j)}{C(i) + C(j)}$ $C(i,j)$: the number of images have two label at same time $C(i)/C(j)$: the number of images in class i/j.

5. Discussion and future direction

The rapid growth of GCNs^{12, 95, 106} and their extensions have been increasingly utilized for processing, integrating, and analyzing multi-modality medical imaging and other types of biological data^{117, 118}. We here discuss several future research directions and common challenges to advance the research in medical image analysis and related research fields. We particularly outline key aspects of importance, including GCN model interpretation, the value of pre-training model, evaluation pipeline, large-scale benchmark, and emerging technical insights.

5.1 Interpretability

The interpretation of GCNs is of heightened interest to make the outcome understandable, ensure model validity, and enhance clinical relevance. In our focus, a well-designed interpretation framework of GCNs is expected to provide the explanation and visualization for both image-wise and graph components understanding. Such an interpretative ability can be highly attractive to clinicians in the process of diagnosing regions of interest in histopathology, enabling an understanding of spatial and regional interactions from graph structures¹². As demonstrated, three metrics are useful to design and understand the interpretation capability of GCNs¹¹⁹: (1) Fidelity refers to the importance of classification as measured by the impact of node attributes, (2) Contrastively points to the significance with respect to different classes, and (3) Sparsity reflects the sparseness level on a graph. These metrics can help generate and measure the valuable heat maps of graph nodes given their attributes. Representative approaches include gradient class activation mapping (Grad-CAM), contrastive excitation backpropagation (c-EB), and contrastive gradient (CG)¹²⁰. Further, we recognize that emerging studies have explored the specified interpretation strategy for GCNs^{98, 99}. For instance, an ROI-selection pooling layer (R-pool)¹¹⁹ highlights the node importance for predicting neurological disorders by removing noisy nodes to realize a dimension reduction of the entire graph. Rather than node-level feature interpretation, additional efforts will be greatly needed on interpreting the relational information in graphs. GnnExplainer⁹⁹ is an example to leverage the recursive neighborhood-aggregation scheme to identify graph pathways as well as node feature information passing along the edges. The design of GnnExplainer is appealing to visualize the detailed cell-graph structure and provide class-specific interpretation for breast cancer⁹⁸. As a result, we strongly emphasize that the interpretation process considers an in-depth joint understanding of the clinical task, graph model architecture, and model performance.

5.2 Model pretraining

Pretraining GCNs aims to train a model on the tasks with a sufficient amount of data and labels and finetune the model into downstream tasks. Pre-trained GCNs can serve as a foundation model to improve the generalization power when the size of the training set is often limited in medical imaging¹²¹. The pretraining workflow of GCNs typically includes the model training rules, hyper-parameter settings, and constructed-graph augmentation strategies. A key pretraining scheme for a graph-level task is to reconstruct the vertex adjacency

information (e.g. GraphSAGE²¹) without hurting intrinsic structural information¹²². We offer several compelling directions of pretraining strategy to improve GCNs model robustness and their utility in different tasks. First, the graph-wise augmentation strategies have a large room to facilitate the pretraining of graphs. For instance, the out-of-distribution samples can be analyzed via node-level and graph-level augmentations^{121, 122}. Second, exploring label-efficient models (e.g., unsupervised or self-supervised learning) in conjunction with pretraining strategies¹²² could greatly alleviate the labeling shortage. Notable studies^{121, 122, 123} have achieved good performance in downstream tasks while leveraging the graph-based pretraining strategies. Considering the above directions, a self-supervised learning framework for GCNs pretraining¹²² demonstrates that graph-wise augmentation strategies are useful to address the graph data heterogeneity. The pretraining is performed through maximizing the agreement between two augmented views of the same graph via performing node dropping, edge perturbation, attribute masking, and subgraph selection. Notably, only a small partition of graph components will be changed, meanwhile the semantic meaning of the graph has been preserved. Such a strategy brings graph data diversity that is greatly needed for building robust pre-trained GCN models. Taken together, the research on pretraining GCNs and their practical impact is only to start and will continue to make progress on downstream image-related clinical tasks.

5.3 Evaluation of graph construction strategies

The evaluation of graph construction in medical imaging is vital because the associated graph construction could significantly affect the model performance and the interpretation of outcomes. The general graph construction methods used ROIs (e.g., image patches or brain neurons) as graph nodes and the node attributes are obtained by standard feature extractors (e.g., ResNet18). In addition, edges represent the connections between nodes which could be determined by the Euclidean distance between node features, or the connections between ROIs which are determined by patch coordinates or the actual neural fiber connections. Currently, graph construction strategies are applied in different tasks and a generalized graph construction evaluation strategy is not explicitly developed yet. It is even more difficult to determine which kind of graph construction is generalizable for task-specific medical image analysis because of various datasets and graph construction metrics. Also, developing a generalized graph construction evaluation strategy is necessary for GCNs to better process medical image data across multiple modalities because the model performance is highly related to the quality of constructed graph-structured data. The benchmarking framework^{124, 125} has rigorously evaluated the performance of graph neural networks on medium-scale datasets and demonstrates its usefulness for analyzing message-passing capability in GCNs. Also, a comparison strategy among multiple GCNs¹²⁵ can address the issues of reproducibility and replicability. Following the graph evaluation^{124, 125}, we need to define statistical distinctions to ensure the performance of GCNs. For example, it is helpful for model training and human understanding if the graph structure and feature distribution differences between positive and negative patient samples are significantly different.

5.4 Real-world large-scale graph benchmark

Despite the remarkable effort on standardization of medical imaging cohorts, the high-quality, large-scale graph-defined benchmark has not been readily available for AI model evaluation, especially in medical image analysis. Open Graph Benchmark (OGB) exemplifies the initiative that contains a diverse set of real-world benchmark datasets (e.g., protein, drug, and molecular elements) to facilitate scalable and reproducible graph machine learning research¹²⁶. The number of graphs and nodes in each graph are both massive in OGB. Even small-scale OGB graphs can have more than 100 thousand nodes or more than 1 million edges. This comprehensive dataset in various domains can be viewed as a baseline to support the GCNs' development and comparison. Related works have been explored on graphs including a chemistry dataset with 2 million graphs and a biology dataset with 395K graphs¹²¹. As seen in OGB development, there are challenges to collecting and processing suitable medical image datasets and constructing meaningful graphs following the image-to-graph transformation. First, we need to collect a large number of medical images across multiple centers to ensure data diversity. It is also essential to provide detailed annotation information for collected datasets on the image-level region of interest. Second, graph-wise statistics is important to allow measurement of graph-level dynamics. Notable graph metrics¹²⁷, such as the average node degree, clustering coefficient, closeness centrality, and betweenness centrality, can be used to assess graph characteristics and help determine unique graph structures. For instance, the average node degree calculates the average degree of the neighborhood of each node to delineate the connectivity between nodes to their neighbors. The clustering coefficient measures how many nodes in the graph tend to cluster together. Closeness centrality highlights nodes that can easily access other nodes. Third, we must carefully design image-graph components, such as the definition of graph nodes in different types of graphs that are vital to downstream clinical tasks. Finally, the real impact of pre-trained foundation models on large-scale graph-wise datasets still needs to be explored. While using pretraining GCNs to improve data-efficiency issues in medical image analysis, the models can be well-trained on the large-scale graph-wise dataset and adapt into specific tasks, even with a limited size of downstream data.

5.5 Technological advancements

The rapid development of deep learning is bringing novel perspectives to address the challenges of graph-based image analysis. The transformer architecture²³, emphasizing the use of a self-attention mechanism to explore long-range sequential knowledge, emerges to improve the model performance in a variety of natural language processing (NLP)¹²⁸ and computer vision tasks^{129, 130}. A graph-wise transformer can be effectively considered to capture both local and global contexts, thus holding the promise to overcome the limitation of spatial-temporal graph convolutions. For example, graph convolutional skeleton transformers integrate both dynamical attention and global context, as well as local topology structure in GCNs¹³¹ while the spatial transformer attention module discovers the global correlations between the bone-connected and the approximated connected joints of graph topology. In medical image analysis, the combination of GCNs and transformer models can be favored to process 3D MRI sequences to boost the model prediction performance,

where GCNs explore the topological features while Transformers could model the temporal relationship among MRI sequences. In the meantime, self-supervised learning strategy is emerging in graph-driven analysis with limited availability of imaging data. Notably, self-supervised learning (SSL) provides a means to pretrain a model with unlabeled data, followed by fine-tuning the model for a downstream task with limited annotations¹³². Contrastive learning (CL), as a particular variant of SSL, introduces a contrastive loss to enforce representations to be close for similar pairs and far for dissimilar pairs^{132,133}. Another technique to address the limitation of data labeling is the advent of self-training learning to generate pseudo-label for model retraining and optimization¹³⁴. A self-training method for MRI segmentation has shown the potential solution for cross-scanner and cross-center data analytical tasks¹³⁴. Also, the teacher-student framework is another type of self-training, which trains a good teacher model with labeled data to annotate the unlabeled data, and finally, the labeled data and data with pseudo-labels can jointly train a student model¹³¹. Overall, both self-supervised learning and self-training strategies can be utilized in GCNs model training to potentially improve the model performance and overcome the annotation and data scale challenges.

6. Conclusion

We have witnessed a growing trend of graph convolutional networks applied to medical image analysis over the past few years. The convergence of GCNs and medical imaging data brings advances into outcome interpretation, disease understanding, and novel insights into data-driven model assessment. These breakthroughs, together with data fusion ability, local and global feature inference, and model training efficiency, lead to a wide range of applications across clinical imaging fields. Nevertheless, the development of benchmark graph-based medical datasets is yet to be established. Consistency and validity of graph construction strategy in medical imaging are greatly needed in future research. Recent technological advances can be considered to enhance and optimize GCNs in addressing challenging problems. We hope that the gleaned insights of this review will serve as a guideline for researchers on graph-driven deep learning across medical imaging disciplines, and will inspire continued efforts on data-driven biomedical research and healthcare applications.

Reference

1. Zhou J, *et al.* Graph neural networks: A review of methods and applications. *AI Open* **1**, 57-81 (2020).
2. Bruna J, Zaremba W, Szlam A, LeCun Y. Spectral networks and locally connected networks on graphs. *arXiv preprint arXiv:13126203*, (2013).
3. Wu Z, Pan S, Chen F, Long G, Zhang C, Philip SY. A comprehensive survey on graph neural networks. *IEEE transactions on neural networks and learning systems* **32**, 4-24 (2020).
4. Zhang S, Tong H, Xu J, Maciejewski R. Graph convolutional networks: a comprehensive review. *Computational Social Networks* **6**, 1-23 (2019).
5. Failmezger H, Muralidhar S, Rullan A, de Andrea CE, Sahai E, Yuan Y. Topological Tumor Graphs: a graph-based spatial model to infer stromal recruitment for immunosuppression in melanoma histology. *Cancer research* **80**, 1199-1209 (2020).
6. Adnan M, Kalra S, Tizhoosh HR. Representation learning of histopathology images using graph neural networks. In: *Proceedings of the IEEE/CVF Conference on Computer Vision and Pattern Recognition Workshops* (2020).
7. Anklin V, *et al.* Learning Whole-Slide Segmentation from Inexact and Incomplete Labels using Tissue Graphs. *arXiv preprint arXiv:210303129*, (2021).
8. Raju A, Yao J, Haq MM, Jonnagaddala J, Huang J. Graph attention multi-instance learning for accurate colorectal cancer staging. In: *International Conference on Medical Image Computing and Computer-Assisted Intervention*. Springer (2020).
9. Perozzi B, Al-Rfou R, Skiena S. Deepwalk: Online learning of social representations. In: *Proceedings of the 20th ACM SIGKDD international conference on Knowledge discovery and data mining* (2014).
10. Grover A, Leskovec J. node2vec: Scalable feature learning for networks. In: *Proceedings of the 22nd ACM SIGKDD international conference on Knowledge discovery and data mining* (2016).
11. Huang Y, Chung AC. Edge-variational graph convolutional networks for uncertainty-aware disease prediction. In: *International Conference on Medical Image Computing and Computer-Assisted Intervention*. Springer (2020).
12. Ding K, Liu Q, Lee E, Zhou M, Lu A, Zhang S. Feature-Enhanced Graph Networks for Genetic Mutational Prediction Using Histopathological Images in Colon Cancer. In: *International Conference on Medical Image Computing and Computer-Assisted Intervention*. Springer (2020).
13. Qu H, *et al.* Genetic mutation and biological pathway prediction based on whole slide images in breast carcinoma using deep learning. *NPJ precision oncology* **5**, 1-11 (2021).

14. Defferrard M, Bresson X, Vandergheynst P. Convolutional neural networks on graphs with fast localized spectral filtering. *Advances in neural information processing systems* **29**, 3844-3852 (2016).
15. Levie R, Monti F, Bresson X, Bronstein MM. Cayleynets: Graph convolutional neural networks with complex rational spectral filters. *IEEE Transactions on Signal Processing* **67**, 97-109 (2018).
16. Kipf TN, Welling M. Semi-supervised classification with graph convolutional networks. *arXiv preprint arXiv:160902907*, (2016).
17. Li R, Wang S, Zhu F, Huang J. Adaptive graph convolutional neural networks. In: *Proceedings of the AAAI Conference on Artificial Intelligence* (2018).
18. Zhuang C, Ma Q. Dual graph convolutional networks for graph-based semi-supervised classification. In: *Proceedings of the 2018 World Wide Web Conference* (2018).
19. Gilmer J, Schoenholz SS, Riley PF, Vinyals O, Dahl GE. Neural message passing for quantum chemistry. In: *International conference on machine learning*. PMLR (2017).
20. Hamilton WL, Ying R, Leskovec J. Inductive representation learning on large graphs. In: *Proceedings of the 31st International Conference on Neural Information Processing Systems* (2017).
21. Xu K, Hu W, Leskovec J, Jegelka S. How powerful are graph neural networks? *arXiv preprint arXiv:181000826*, (2018).
22. Veličković P, Cucurull G, Casanova A, Romero A, Lio P, Bengio Y. Graph attention networks. *arXiv preprint arXiv:171010903*, (2017).
23. Vaswani A, et al. Attention is all you need. In: *Advances in neural information processing systems* (2017).
24. Scarselli F, Gori M, Tsoi AC, Hagenbuchner M, Monfardini G. The graph neural network model. *IEEE transactions on neural networks* **20**, 61-80 (2008).
25. Liu M, Gao H, Ji S. Towards deeper graph neural networks. In: *Proceedings of the 26th ACM SIGKDD International Conference on Knowledge Discovery & Data Mining* (2020).
26. Kearnes S, McCloskey K, Berndl M, Pande V, Riley P. Molecular graph convolutions: moving beyond fingerprints. *Journal of computer-aided molecular design* **30**, 595-608 (2016).
27. Pham T, Tran T, Phung D, Venkatesh S. Column networks for collective classification. In: *Thirty-first AAAI conference on artificial intelligence* (2017).
28. Simonovsky M, Komodakis N. Dynamic edge-conditioned filters in convolutional neural networks on graphs. In: *Proceedings of the IEEE conference on computer vision and pattern recognition* (2017).

29. Atwood J, Towsley D. Diffusion-convolutional neural networks. In: *Advances in neural information processing systems*) (2016).
30. Li Y, Yu R, Shahabi C, Liu Y. Diffusion convolutional recurrent neural network: Data-driven traffic forecasting. *arXiv preprint arXiv:170701926*, (2017).
31. Derr T, Ma Y, Tang J. Signed graph convolutional networks. In: *2018 IEEE International Conference on Data Mining (ICDM)*. IEEE (2018).
32. Such FP, *et al.* Robust spatial filtering with graph convolutional neural networks. *IEEE Journal of Selected Topics in Signal Processing* **11**, 884-896 (2017).
33. Wang X, *et al.* Heterogeneous graph attention network. In: *The World Wide Web Conference*) (2019).
34. Mesquita D, Souza AH, Kaski S. Rethinking pooling in graph neural networks. *arXiv preprint arXiv:201011418*, (2020).
35. Zhang M, Cui Z, Neumann M, Chen Y. An end-to-end deep learning architecture for graph classification. In: *Thirty-Second AAAI Conference on Artificial Intelligence*) (2018).
36. Li Y, Tarlow D, Brockschmidt M, Zemel R. Gated graph sequence neural networks. *arXiv preprint arXiv:151105493*, (2015).
37. Bianchi FM, Grattarola D, Alippi C. Mincut pooling in graph neural networks. (2019).
38. Ying R, You J, Morris C, Ren X, Hamilton WL, Leskovec J. Hierarchical graph representation learning with differentiable pooling. *arXiv preprint arXiv:180608804*, (2018).
39. Cangea C, Veličković P, Jovanović N, Kipf T, Liò P. Towards sparse hierarchical graph classifiers. *arXiv preprint arXiv:181101287*, (2018).
40. Gao H, Ji S. Graph u-nets. In: *international conference on machine learning*). PMLR (2019).
41. Knyazev B, Taylor GW, Amer MR. Understanding attention and generalization in graph neural networks. *arXiv preprint arXiv:190502850*, (2019).
42. Lee J, Lee I, Kang J. Self-attention graph pooling. In: *International Conference on Machine Learning*). PMLR (2019).
43. Diehl F, Brunner T, Le MT, Knoll A. Towards graph pooling by edge contraction. In: *ICML 2019 Workshop on Learning and Reasoning with Graph-Structured Data*) (2019).
44. Diehl F. Edge contraction pooling for graph neural networks. *arXiv preprint arXiv:190510990*, (2019).
45. Chen D, Lin Y, Li W, Li P, Zhou J, Sun X. Measuring and relieving the over-smoothing problem for graph neural networks from the topological view. In: *Proceedings of the AAAI Conference on Artificial Intelligence*) (2020).

46. Li Q, Han Z, Wu X-M. Deeper insights into graph convolutional networks for semi-supervised learning. In: *Thirty-Second AAAI conference on artificial intelligence* (2018).
47. Xu K, Li C, Tian Y, Sonobe T, Kawarabayashi K-i, Jegelka S. Representation learning on graphs with jumping knowledge networks. In: *International Conference on Machine Learning*. PMLR (2018).
48. Ibragimov B, Xing L. Segmentation of organs - at - risks in head and neck CT images using convolutional neural networks. *Medical physics* **44**, 547-557 (2017).
49. Havaei M, *et al.* Brain tumor segmentation with deep neural networks. *Medical image analysis* **35**, 18-31 (2017).
50. Chilamkurthy S, *et al.* Deep learning algorithms for detection of critical findings in head CT scans: a retrospective study. *The Lancet* **392**, 2388-2396 (2018).
51. Grewal M, Srivastava MM, Kumar P, Varadarajan S. Radnet: Radiologist level accuracy using deep learning for hemorrhage detection in ct scans. In: *2018 IEEE 15th International Symposium on Biomedical Imaging (ISBI 2018)*. IEEE (2018).
52. Lakshmanaprabu S, Mohanty SN, Shankar K, Arunkumar N, Ramirez G. Optimal deep learning model for classification of lung cancer on CT images. *Future Generation Computer Systems* **92**, 374-382 (2019).
53. Frid-Adar M, Klang E, Amitai M, Goldberger J, Greenspan H. Synthetic data augmentation using GAN for improved liver lesion classification. In: *2018 IEEE 15th international symposium on biomedical imaging (ISBI 2018)*. IEEE (2018).
54. Ktena SI, *et al.* Metric learning with spectral graph convolutions on brain connectivity networks. *NeuroImage* **169**, 431-442 (2018).
55. Zhang Y, Zhan L, Cai W, Thompson P, Huang H. Integrating heterogeneous brain networks for predicting brain disease conditions. In: *International Conference on Medical Image Computing and Computer-Assisted Intervention*. Springer (2019).
56. Burwinkel H, *et al.* Adaptive image-feature learning for disease classification using inductive graph networks. In: *International Conference on Medical Image Computing and Computer-Assisted Intervention*. Springer (2019).
57. Kong Y, Gao J, Xu Y, Pan Y, Wang J, Liu J. Classification of autism spectrum disorder by combining brain connectivity and deep neural network classifier. *Neurocomputing* **324**, 63-68 (2019).
58. Logothetis NK, Pauls J, Augath M, Trinath T, Oeltermann A. Neurophysiological investigation of the basis of the fMRI signal. *nature* **412**, 150-157 (2001).
59. Seeman P, Madras B. *Imaging of the human brain in health and disease*. Elsevier (2013).
60. Narayan R. *Encyclopedia of biomedical engineering*. Elsevier (2018).

61. Korolev S, Safiullin A, Belyaev M, Dodonova Y. Residual and plain convolutional neural networks for 3D brain MRI classification. In: *2017 IEEE 14th international symposium on biomedical imaging (ISBI 2017)*. IEEE (2017).
62. Sporns O. Contributions and challenges for network models in cognitive neuroscience. *Nature neuroscience* **17**, 652-660 (2014).
63. Shen W, Zhou M, Yang F, Yang C, Tian J. Multi-scale convolutional neural networks for lung nodule classification. In: *International conference on information processing in medical imaging*. Springer (2015).
64. Shen W, *et al.* Multi-crop convolutional neural networks for lung nodule malignancy suspiciousness classification. *Pattern Recognition* **61**, 663-673 (2017).
65. Wang S, *et al.* Central focused convolutional neural networks: Developing a data-driven model for lung nodule segmentation. *Medical image analysis* **40**, 172-183 (2017).
66. Tzourio-Mazoyer N, *et al.* Automated anatomical labeling of activations in SPM using a macroscopic anatomical parcellation of the MNI MRI single-subject brain. *Neuroimage* **15**, 273-289 (2002).
67. Zalesky A, *et al.* Whole-brain anatomical networks: does the choice of nodes matter? *Neuroimage* **50**, 970-983 (2010).
68. Liu C, *et al.* Computational network biology: data, models, and applications. *Physics Reports* **846**, 1-66 (2020).
69. Li X, Dvornek NC, Zhou Y, Zhuang J, Ventola P, Duncan JS. Graph neural network for interpreting task-fMRI biomarkers. In: *International Conference on Medical Image Computing and Computer-Assisted Intervention*. Springer (2019).
70. Di Martino A, *et al.* The autism brain imaging data exchange: towards a large-scale evaluation of the intrinsic brain architecture in autism. *Molecular psychiatry* **19**, 659-667 (2014).
71. Sudlow C, *et al.* UK biobank: an open access resource for identifying the causes of a wide range of complex diseases of middle and old age. *PLoS medicine* **12**, e1001779 (2015).
72. Koch G, Zemel R, Salakhutdinov R. Siamese neural networks for one-shot image recognition. In: *ICML deep learning workshop*. Lille (2015).
73. Achard S, Salvador R, Whitcher B, Suckling J, Bullmore E. A resilient, low-frequency, small-world human brain functional network with highly connected association cortical hubs. *Journal of Neuroscience* **26**, 63-72 (2006).
74. van der Horn HJ, Liemburg EJ, Scheenen ME, de Koning ME, Spikman JM, van der Naalt J. Graph analysis of functional brain networks in patients with mild traumatic brain injury. *PLoS One* **12**, e0171031 (2017).
75. Kabbara A, Falou WE, Khalil M, Wendling F, Hassan M. Graph analysis of spontaneous brain network using EEG source connectivity. *arXiv preprint arXiv:160700952*, (2016).

76. Marek K, *et al.* The Parkinson progression marker initiative (PPMI). *Progress in neurobiology* **95**, 629-635 (2011).
77. Chen G, *et al.* Estimating Tissue Microstructure with Undersampled Diffusion Data via Graph Convolutional Neural Networks. In: *International Conference on Medical Image Computing and Computer-Assisted Intervention*. Springer (2020).
78. Yang H, *et al.* Interpretable multimodality embedding of cerebral cortex using attention graph network for identifying bipolar disorder. In: *International Conference on Medical Image Computing and Computer-Assisted Intervention*. Springer (2019).
79. Liu J, Ma G, Jiang F, Lu C-T, Philip SY, Ragin AB. Community-preserving graph convolutions for structural and functional joint embedding of brain networks. In: *2019 IEEE International Conference on Big Data (Big Data)*. IEEE (2019).
80. Zhai Z, *et al.* Linking convolutional neural networks with graph convolutional networks: application in pulmonary artery-vein separation. In: *International Workshop on Graph Learning in Medical Imaging*. Springer (2019).
81. Saha P, Mukherjee D, Singh PK, Ahmadian A, Ferrara M, Sarkar R. GraphCovidNet: A graph neural network based model for detecting COVID-19 from CT scans and X-rays of chest. *Scientific reports* **11**, (2021).
82. Rajpurkar P, *et al.* Chexnet: Radiologist-level pneumonia detection on chest x-rays with deep learning. *arXiv preprint arXiv:171105225*, (2017).
83. De Matos J, Britto Jr AdS, Oliveira LE, Koerich AL. Histopathologic image processing: A review. *arXiv preprint arXiv:190407900*, (2019).
84. Gurcan MN, Boucheron LE, Can A, Madabhushi A, Rajpoot NM, Yener B. Histopathological image analysis: A review. *IEEE reviews in biomedical engineering* **2**, 147-171 (2009).
85. Zhou X, *et al.* A comprehensive review for breast histopathology image analysis using classical and deep neural networks. *IEEE Access* **8**, 90931-90956 (2020).
86. Zhou Y, Graham S, Alemi Koohbanani N, Shaban M, Heng P-A, Rajpoot N. Cgc-net: Cell graph convolutional network for grading of colorectal cancer histology images. In: *Proceedings of the IEEE/CVF International Conference on Computer Vision Workshops* (2019).
87. Anand D, Gadiya S, Sethi A. Histograms: graphs in histopathology. In: *Medical Imaging 2020: Digital Pathology*. International Society for Optics and Photonics (2020).
88. Keenan SJ, *et al.* An automated machine vision system for the histological grading of cervical intraepithelial neoplasia (CIN). *The Journal of pathology* **192**, 351-362 (2000).
89. Bilgin C, Demir C, Nagi C, Yener B. Cell-graph mining for breast tissue modeling and classification. In: *2007 29th Annual International Conference of the IEEE Engineering in Medicine and Biology Society*. IEEE (2007).

90. Sandler M, Howard A, Zhu M, Zhmoginov A, Chen L-C. Mobilenetv2: Inverted residuals and linear bottlenecks. In: *Proceedings of the IEEE conference on computer vision and pattern recognition* (2018).
91. Potjer FK. Region adjacency graphs and connected morphological operators. In: *Mathematical Morphology and Its Applications to Image and Signal Processing*. Springer (1996).
92. Xue Y, Xu T, Huang X. Adversarial learning with multi-scale loss for skin lesion segmentation. In: *2018 IEEE 15th International Symposium on Biomedical Imaging (ISBI 2018)*. IEEE (2018).
93. Wang G, Song T, Dong Q, Cui M, Huang N, Zhang S. Automatic ischemic stroke lesion segmentation from computed tomography perfusion images by image synthesis and attention-based deep neural networks. *Medical Image Analysis* **65**, 101787 (2020).
94. Qu H, *et al.* Weakly supervised deep nuclei segmentation using partial points annotation in histopathology images. *IEEE Transactions on Medical Imaging* **39**, 3655-3666 (2020).
95. Zhao Y, *et al.* Predicting lymph node metastasis using histopathological images based on multiple instance learning with deep graph convolution. In: *Proceedings of the IEEE/CVF Conference on Computer Vision and Pattern Recognition* (2020).
96. Larsen ABL, Sønderby SK, Larochelle H, Winther O. Autoencoding beyond pixels using a learned similarity metric. In: *International conference on machine learning*. PMLR (2016).
97. Levy J, Haudenschild C, Barwick C, Christensen B, Vaickus L. Topological feature extraction and visualization of whole slide images using graph neural networks. In: *BIOCOMPUTING 2021: Proceedings of the Pacific Symposium*. World Scientific (2020).
98. Jaume G, *et al.* Towards explainable graph representations in digital pathology. *arXiv preprint arXiv:200700311*, (2020).
99. Ying R, Bourgeois D, You J, Zitnik M, Leskovec J. Gnnexplainer: Generating explanations for graph neural networks. *Advances in neural information processing systems* **32**, 9240 (2019).
100. Sureka M, Patil A, Anand D, Sethi A. Visualization for histopathology images using graph convolutional neural networks. In: *2020 IEEE 20th International Conference on Bioinformatics and Bioengineering (BIBE)*. IEEE (2020).
101. Pati P, *et al.* Hact-net: A hierarchical cell-to-tissue graph neural network for histopathological image classification. In: *Uncertainty for Safe Utilization of Machine Learning in Medical Imaging, and Graphs in Biomedical Image Analysis*. Springer (2020).
102. Kumar N, Verma R, Sharma S, Bhargava S, Vahadane A, Sethi A. A dataset and a technique for generalized nuclear segmentation for computational pathology. *IEEE transactions on medical imaging* **36**, 1550-1560 (2017).

103. Graham S, *et al.* Hover-net: Simultaneous segmentation and classification of nuclei in multi-tissue histology images. *Medical Image Analysis* **58**, 101563 (2019).
104. Bodnar C, Cangea C, Lio P. Deep graph mapper: Seeing graphs through the neural lens. *arXiv preprint arXiv:200203864*, (2020).
105. Wang Y, *et al.* Cell graph neural networks enable digital staging of tumour microenvironment and precisely predict patient survival in gastric cancer. *medRxiv*, (2021).
106. Li R, Yao J, Zhu X, Li Y, Huang J. Graph CNN for survival analysis on whole slide pathological images. In: *International Conference on Medical Image Computing and Computer-Assisted Intervention*. Springer (2018).
107. Wang Z, *et al.* Hierarchical Graph Pathomic Network for Progression Free Survival Prediction. In: *International Conference on Medical Image Computing and Computer-Assisted Intervention*. Springer (2021).
108. He K, Gkioxari G, Dollár P, Girshick R. Mask r-cnn. In: *Proceedings of the IEEE international conference on computer vision* (2017).
109. Kather JN, *et al.* Deep learning can predict microsatellite instability directly from histology in gastrointestinal cancer. *Nature medicine* **25**, 1054-1056 (2019).
110. Kather JN, *et al.* Pan-cancer image-based detection of clinically actionable genetic alterations. *Nature cancer* **1**, 789-799 (2020).
111. Fu Y, *et al.* Pan-cancer computational histopathology reveals mutations, tumor composition and prognosis. *Nature Cancer* **1**, 800-810 (2020).
112. Lu W, Graham S, Bilal M, Rajpoot N, Minhas F. Capturing Cellular Topology in Multi-Gigapixel Pathology Images. In: *Proceedings of the IEEE/CVF Conference on Computer Vision and Pattern Recognition Workshops* (2020).
113. Müllner D. Modern hierarchical, agglomerative clustering algorithms. *arXiv preprint arXiv:11092378*, (2011).
114. Shin SY, Lee S, Yun ID, Lee KM. Deep vessel segmentation by learning graphical connectivity. *Medical image analysis* **58**, 101556 (2019).
115. Noh KJ, Park SJ, Lee S. Combining fundus images and fluorescein angiography for artery/vein classification using the hierarchical vessel graph network. In: *International Conference on Medical Image Computing and Computer-Assisted Intervention*. Springer (2020).
116. Wu J, *et al.* Learning Differential Diagnosis of Skin Conditions with Co-occurrence Supervision Using Graph Convolutional Networks. In: *International Conference on Medical Image Computing and Computer-Assisted Intervention*. Springer (2020).
117. Liu Q, Hu Z, Jiang R, Zhou M. DeepCDR: a hybrid graph convolutional network for predicting cancer drug response. *Bioinformatics* **36**, i911-i918 (2020).

118. Wang Z, Zhou M, Arnold C. Toward heterogeneous information fusion: bipartite graph convolutional networks for in silico drug repurposing. *Bioinformatics* **36**, i525-i533 (2020).
119. Li X, *et al.* Braingnn: Interpretable brain graph neural network for fmri analysis. *Medical Image Analysis* **74**, 102233 (2021).
120. Pope PE, Kolouri S, Rostami M, Martin CE, Hoffmann H. Explainability methods for graph convolutional neural networks. In: *Proceedings of the IEEE/CVF Conference on Computer Vision and Pattern Recognition* (2019).
121. Hu W, *et al.* Strategies for pre-training graph neural networks. *arXiv preprint arXiv:190512265*, (2019).
122. You Y, Chen T, Sui Y, Chen T, Wang Z, Shen Y. Graph contrastive learning with augmentations. *Advances in Neural Information Processing Systems* **33**, 5812-5823 (2020).
123. Qiu J, *et al.* Gcc: Graph contrastive coding for graph neural network pre-training. In: *Proceedings of the 26th ACM SIGKDD International Conference on Knowledge Discovery & Data Mining* (2020).
124. Dwivedi VP, Joshi CK, Laurent T, Bengio Y, Bresson X. Benchmarking graph neural networks. *arXiv preprint arXiv:200300982*, (2020).
125. Errica F, Podda M, Bacciu D, Micheli A. A fair comparison of graph neural networks for graph classification. *arXiv preprint arXiv:191209893*, (2019).
126. Hu W, *et al.* Open graph benchmark: Datasets for machine learning on graphs. *arXiv preprint arXiv:200500687*, (2020).
127. Zamanitajeddin N, Jahanifar M, Rajpoot N. Cells are actors: Social network analysis with classical ml for sota histology image classification. In: *International Conference on Medical Image Computing and Computer-Assisted Intervention*. Springer (2021).
128. Devlin J, Chang M-W, Lee K, Toutanova K. Bert: Pre-training of deep bidirectional transformers for language understanding. *arXiv preprint arXiv:181004805*, (2018).
129. Gao Y, Zhou M, Metaxas DN. UTNet: a hybrid transformer architecture for medical image segmentation. In: *International Conference on Medical Image Computing and Computer-Assisted Intervention*. Springer (2021).
130. Dosovitskiy A, *et al.* An image is worth 16x16 words: Transformers for image recognition at scale. *arXiv preprint arXiv:201011929*, (2020).
131. Bai R, *et al.* GCsT: Graph Convolutional Skeleton Transformer for Action Recognition. *arXiv preprint arXiv:210902860*, (2021).
132. Chaitanya K, Erdil E, Karani N, Konukoglu E. Contrastive learning of global and local features for medical image segmentation with limited annotations. *arXiv preprint arXiv:200610511*, (2020).

133. Xie Q, Luong M-T, Hovy E, Le QV. Self-training with noisy student improves imagenet classification. In: *Proceedings of the IEEE/CVF Conference on Computer Vision and Pattern Recognition* (2020).
134. Liu X, et al. Generative self-training for cross-domain unsupervised tagged-to-cine mri synthesis. In: *International Conference on Medical Image Computing and Computer-Assisted Intervention*. Springer (2021).